(0.20 mM) for 5 days. The cell proliferation assay showed that the SHya coating suppressed keratinocyte proliferation remarkably in a dose-dependent manner (Fig. 3).

3.3. Effect of SHya coating on keratin1 and loricrin expression

To ensure that the SHya coating promoted keratinocyte differentiation, we detected the relative expression levels of differential marker mRNA by real-time RT-PCR. After NHEKs were incubated with SHya coating in a high-calcium condition (0.20 mM) for 5 days, the expression level of keratin1 mRNA on NHEKs was increased more than eight-fold compared to the control (Fig. 4A) and that of loricrin mRNA was increased in a dose-dependent manner (Fig. 4B).

3.4. Effect of SHya coating on Wnts expressions

The expression levels of Wnt4 and Wnt6 mRNA on NHEKs incubated with SHya coating in the low-calcium condition were measured (Fig. 5A and B); the expression level of Wnt5a of NHEKs incubated with SHya coating was decreased to 95% of the control (Fig. 5C) and that of Wnt7a mRNA to about 40% of the control (Fig. 5D).

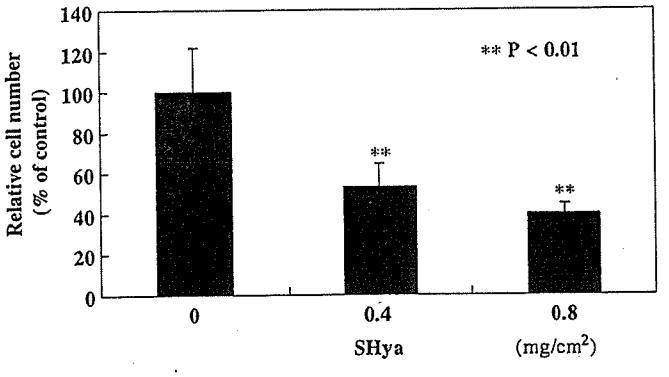

Fig. 3. Suppressive effect of SHya on keratinocyte proliferation. NHEKs were seeded at 1.0×10^4 cells/cm^2 densities onto non-coated (A), 0.4 mg/cm^2 SHya-coated (B), and 0.8 mg/cm^2 SHya-coated (C) 24-well plates and cultured for 5 days. Then numbers of NHEKs were determined by crystal violet assay. Each value is expressed as the mean ± SD. $^{**}P < 0.01$ compared to control.

3.5. Effect of SHya coating on Notch expressions

The expression level of Notch1 mRNA on NHEKs incubated with SHya coating was decreased about 75% compared to the control, and that of Notch2 mRNA was similar to the control (Fig. 6A and B). However, the expression level of Notch3 mRNA was increased about eight-fold compared to the control (Fig. 6C).

4. Discussion

Several studies have suggested that SHya interacts with cells [4], but the effect of SHya on cell differentiation and intercellular signaling was not clear. We demonstrated that a SHya coating promoted keratinocyte differentiation and modulated the expression levels of Notch and Wnt mRNAs.

In this study, the expression levels of Wnt4 and Wnt6 on NHEKs incubated with SHya were increased. A mouse keratinocyte cell line with a deficit of Wnt4 expression showed less differentiation [18]. Wnt6 regulated epithelization [19], suggesting that the SHya-induced upregulation of Wnt4 and Wnt6 is associated with the regulation of keratinocyte differentiation. Wnt7a promoted cell proliferation in corneal epithelial cells during wound healing [20], suggesting that SHya down-regulated Wnt7a expression, resulting in the enhancement of keratinocyte differentiation. The activation of beta-catenin, a downstream factor of Wnt signaling, contributes to keratinocyte differentiation [27]. A sulfated proteoglycan-induced Wnt-11 expression in mouse kidney cells, and sulfated polysaccharides were required in Wnt signaling in mouse kidney cells [28,29]. Therefore, it was suggested

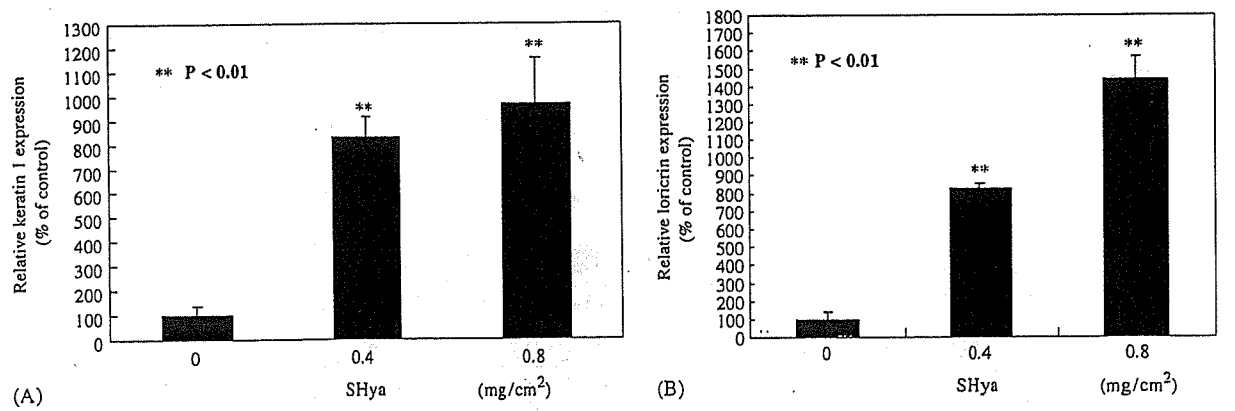

Fig. 4. The expression levels of keratin1 and loricrin mRNA of NHEKs incubated with SHya coating. NHEKs were seeded at 1.0×10^4 cells/cm^2 onto SHya-coated 60 mm dishes (0, 0.4, and 0.8 mg/cm^2) and cultured in medium with 0.20 mM calcium for 5 days. Then RNA was extracted, and real-time RT-PCR was performed to determine the expression levels of keratin1 and loricrin mRNA. Effect of SHya on the expression level of (A) keratin1 mRNA, and (B) loricrin mRNA. Each value is expressed as the mean ± SD. $^{**}P < 0.01$ compared to control.

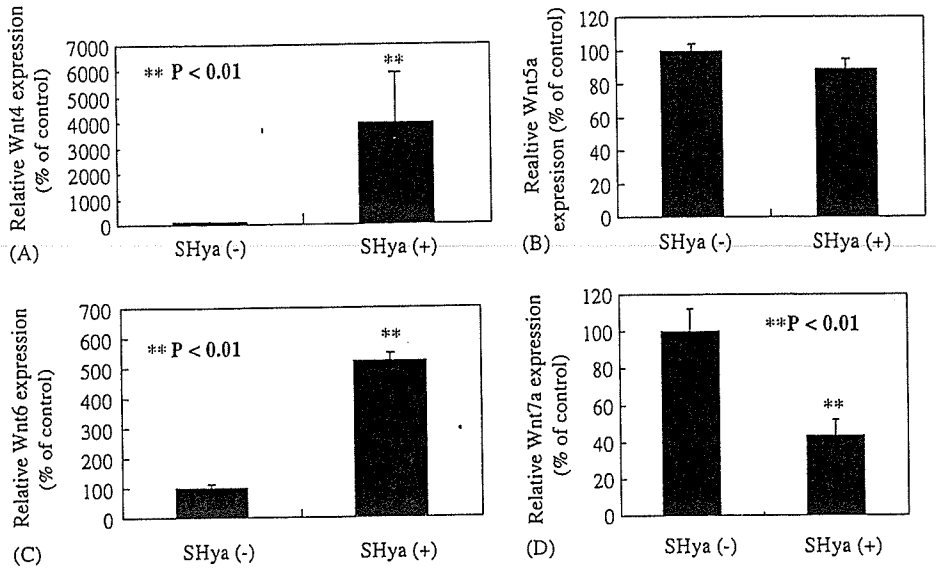

Fig. 5. The expression level of Wnt mRNA in NHEKs incubated with SHya coating. NHEKs were seeded at 1.0×10^4 cells/cm^2 onto SHya-coated 60 mm dishes (0 and 0.8 mg/cm^2) and cultured in medium with 0.20 mM calcium for 20 h. Then RNA was extracted, and real-time RT-PCR was performed to determine the expression level of Wnt mRNA. Effect of SHya on the expression level of (A) Wnt4 mRNA, (B) Wnt5a mRNA, (C) Wnt6 mRNA, and (D) Wnt7a mRNA. Each value is expressed as the mean ± SD. $^{**}P < 0.01$ compared to control.

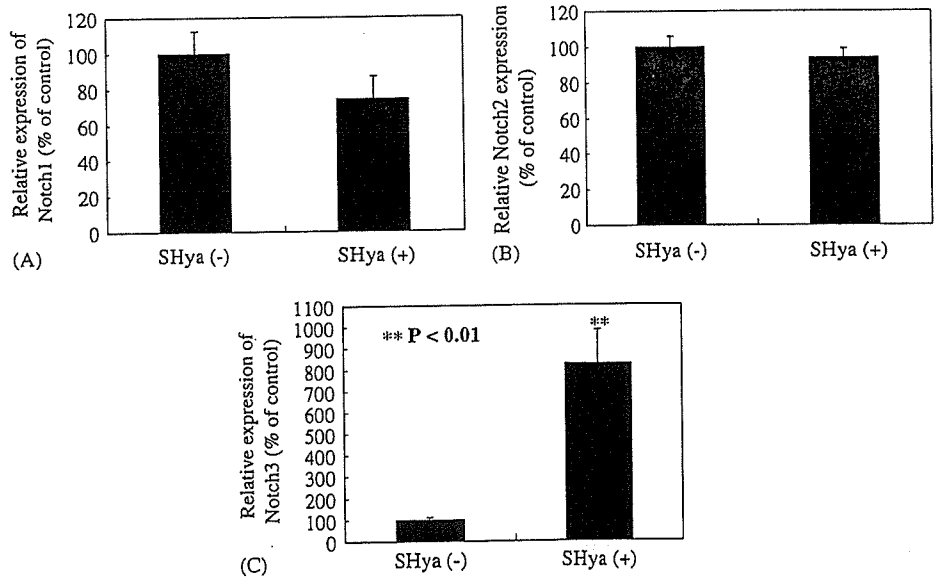

Fig. 6. The expression level of Notch mRNA in NHEKs incubated with SHya coating. NHEKs were seeded at 1.0×10^4 cells/cm^2 onto SHya-coated 60 mm dishes (0, 0.4, and 0.8 mg/cm^2) and cultured in medium with 0.20 mM calcium for 5 days. Then RNA was extracted, and real-time RT-PCR was performed to measure the expression level of notch mRNA. The effect of SHya on the expression level of (A) Notch1 mRNA, (B) Notch2 mRNA, and (C) Notch3 mRNA. Each value is expressed as the mean ± SD. $^{**}P < 0.01$ compared to control.

that SHya modulated Wnt signaling leading to beta-catenin activation.

In mouse keratinocytes, Notch1 is associated with the regulation of cell differentiation via p21, and Notch1 activation down-regulates Wnt4 expression [21]. Notch1 is required in keratinocyte differentiation and in the regulation of Wnt expression [24]. Activation of Notch receptors induces an increase in its own expression level by a positive feedback mechanism [24]. The expression of Notch1 in NHEKs incubated in SHya-coated dishes was decreased compared to that of the control. It was suggested that the decrease in Notch1 expression triggered by SHya induced the increase of Wnt4. The expression level of Notch3 mRNA in NHEKs incubated with SHya coating was increased, suggesting that SHya interacted with Notch3, particularly resulting in the modulation of Wnt expression (Fig. 7). Notch3 is required for the differentiation of vascular smooth muscle cells or T cells [23,24]. The role of Notch3 in keratinocyte differentiation triggered by elevation of the extracellular calcium-ion concentration may not

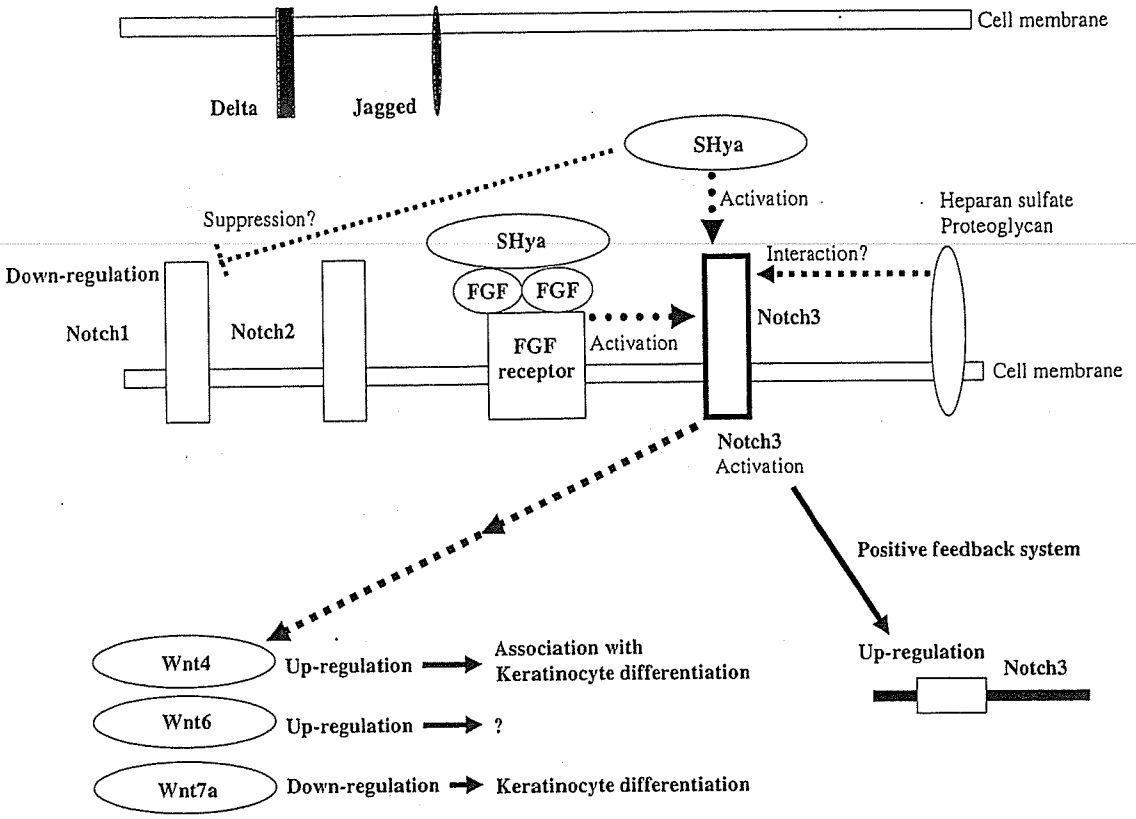

Fig. 7. Diagram of the effect of SHya on Wnt expression via Notch3.

be important, but Notch3 may be activated by SHya, leading to a modulation of intracellular signaling and enhancement of keratinocyte differentiation. Notch3 may be required for interaction with the sulfate groups of sulfated polysaccharides.

Notch1 activation stimulates p21 via the RBP-J kappa transcription factor, resulting in growth arrest, keratinocyte differentiation, or a decrease of Wnt4 expression [25]. Therefore, SHya might activate p21 via Notch3 activation, leading to the modulation of Wnt expression.

The differentiation of NHEKs incubated in SHya was better than that in Hya (data not shown). This suggests that the introduction of sulfate groups into Hya may be a key factor in the enhancement of keratinocyte differentiation.

Normal human dermal fibroblasts showed very low adhesiveness to Hya-coated surfaces because of the anionic surface of Hya [10,11]. However, NHEKs showed very high adhesiveness to SHya-coated surfaces. This suggested that the introduction of sulfate groups into Hya may change the property of its surface, resulting in a high adhesiveness. Sulfated polysaccharides such as heparin and heparan sulfate enhance the stabilities of some growth factors or adsorption of them by the cell membrane, resulting in the enhancement of cell differentiation [13]. The sulfate groups of SHya may bind to and stabilize cationic growth factors, and stabilized growth factors may neutralize the negative charge of the SHya surface, resulting in high cell attachment. Further, it was reported that fibroblast growth factors (FGF) receptors interact with the Notch signaling pathway [30,31]. Therefore, it was suggested that SHya binds and stabilizes FGF to activate FGF receptors leading to stimulation of Notch3 and intercellular signaling.

5. Conclusion

This study demonstrated that a SHya coating promoted keratinocyte differentiation triggered by an elevated extracellular calcium ion concentration. Furthermore, SHya modulated Wnt expressions and increased the expression level of Notch3 mRNA. These results suggest that Notch3 may be an important target for the regulation of cell differentiation. SHya may be a useful biomaterial to regulate Wnt signaling in tissue engineering. This study provides new information that clarifies the interaction between sulfate groups and Notch families. Studies are in progress to clarify the roles of these modulations of *Notch* and *Wnt* genes in keratinocyte differentiation.

Acknowledgments

Special thanks to Dr. Misao Nagahata-Ishiguro for providing sulfated hyaluronan. This work was supported by Health and Labour Sciences Research Grants on Advanced Medical Technology (H14-001) and the Health Sciences focusing on Drug Innovation (KH61059) and on

Human Genome, Tissue Engineering (H17-022), from the Japanese Ministry of Health, Labour and Welfare.

References

[1] Blacker KL, William ML, Goldyne M. Mitomycin C-treated 3T3 fibroblasts used as feeder layers for human keratinocyte culture retain the capacity to generate eicosanoids. J Invest Dermatol 1987;89: 536–9.

[2] Lam PK, Chan ES, Yen RS, Lau HC, King WW. A new system for the cultivation of keratinocytes on acellular human dermis with the use of fibrin glue and 3T3 feeder cells. J Burn Care Rehabil 2000;21:1–4.

[3] Meana A, Iglesias J, Del RM, Larcher F, Madrigal B, Fresno MF, et al. Large surface of cultured human epithelium obtained on a dermal matrix based on live fibroblast-containing fibrin gels. Burns 1998;24:621–30.

[4] Hollander D, Stein M, Bernd A, Windolf J, Wagner R, Pannike A. Autologous keratinocyte culture on hyaluronic acid ester membrane: an alternative in complicated wound management? Unfallchirurgie 1996;22:268–72.

[5] Boyce S, Michel S, Reichert U, Shroot B, Schmidt R. Reconstructed skin from cultured human keratinocytes and fibroblasts on a collagen–glycosaminoglycan biopolymer substrate. Skin Pharmacol 1990;3:136–43.

[6] Lapcik L Jr and L, Lapcik L, De Smedt S, Demeester J, Chabrecek P. Hyaluronan: preparation, structure, properties, and applications. Chem Rev 1998;98:2663–84.

[7] Laurent TC, Fraser JE. Hyaluronan. FASEB J 1992;6:2397–404.

[8] Kimata K, Honma Y, Okayama M, Oguri K, Hozumi M, Suzuki S. Increased synthesis of hyaluronic acid by mouse mammary carcinoma cell variants with high metastatic potential. Cancer Res 1983;43: 1347–54.

[9] Knudson CB, Knudson W. Hyaluronan-binding proteins in development, tissue homeostasis, and disease. FASEB J 1983;7:1233–41.

[10] Park JU, Tsuchiya T. Increase in gap junctional intercellular communication by high molecular weight hyaluronic acid associated with fibroblast growth factor 2 and keratinocyte growth factor production in normal human dermal fibroblasts. Tissue Eng 2002;8: 419–27.

[11] Park JU, Tsuchiya T. Increase in gap-junctional intercellular communications (GJIC) of normal human dermal fibroblasts (NHDF) on surfaces coated with high-molecular-weight hyaluronic acid (HMW HA). J Biomed Mater Res 2002;60:541–7.

[12] Takada T, Katagiri T, Ifuku M, Morimura N, Kobayashi M, Hasegawa K, et al. Sulfated polysaccharides enhance the biological activities of bone morphogenetic proteins. J Biol Chem 2003;278: 43229–35.

[13] Chamow SM, Schwall RH, Stack RJ. Sulphated oligosaccharides promote hepatocyte growth factor association and govern its activity. J Biol Chem 1995;14:16871–8.

[14] Nagahata M, Tsuchiya T, Ishiguro T, Matsuda N, Nakatsuchi Y, Teramoto A, et al. A novel function of *N*-cadherin and connexin43: marked enhancement of alkaline phosphatase activity in rat calvarial osteoblast exposed to sulfated hyaluronan. Biochem Biophys Res Commun 2004;315:603–11.

[15] Kavalkovich KW, Boynton RE, Murphy JM, Barry F. Chondrogenic differentiation of human mesenchymal stem cells within an alginate layer culture system. In Vitro Cell Dev Biol Anim 2002;38:457–66.

[16] Yang R, Yan Z, Chen F, Hansson GK, Kiessling R. Hyaluronic acid and chondroitin sulphate A rapidly promote differentiation of immature DC with upregulation of costimulatory and antigen-presenting molecules, and enhancement of NF-κB and protein kinase activity. Scand J Immunol 2002;55:2–13.

[17] Matsuda M, Shikata K, Shimizu F, Suzuki Y, Miyasaka M, Kawachi H, et al. Therapeutic effect of sulphated hyaluronic acid, a potential selectin-blocking agent, on experimental progressive mesangial proliferative glomerulonephritis. J Pathol 2002;198:407–14.

[18] Saitoh A, Laura A, Vogel HJC, Udey MC. Characterization of *Wnt* gene expression in murine skin: possible involvement of epidermis-derived Wnt-4 in cutaneous epithelial–mesenchymal interactions. Exp Cell Res 1998;243:150–60.

[19] Schmidit C, Stoeckelhuber M, Mckinnell I, Putz R, Christ B, Patel K. Wnt6 regulates the epithelialisation process of the segmental plate mesoderm leading somite formation. Dev Biol 2004;271: 198–209.

[20] Jungmook L, Choun-Ki J. Wnt-7a up-regulates matrix metalloproteinase-12 expression and promotes cell proliferation in corneal epithelial cells during wound healing. J Biol Chem 2005;280: 21653–60.

[21] Rangarajan A, Talora C, Okuyama R, Nicolas M, Mammucari C, Oh H, et al. Notch signaling is a direct determinant of keratinocyte growth arrest and entry into differentiation. EMBO J 2001;20: 3427–36.

[22] Devgan V, Mammucari C, Millar SE, Brisken C, Dotto GP. p21WAF1/Cip1 is a negative transcriptional regulator of Wnt4 expression downstream of Notch1 activation. Genes Dev 2005;19: 1485–95.

[23] Domenga V, Fardoux P, Lacombe P, Monet M, Maciazek J, Krebs LT, et al. *Notch3* is required for arterial identity and maturation of vascular smooth muscle cells. Genes Dev 2004;18:2730–5.

[24] Vacca A, Felli MP, Palermo R, Di Mario G, Calce A, Di Giovine M, et al. Notch3 and pre-TCR interaction unveils distinct NF-kappaB pathways in T-cell development and leukemia. EMBO J 2006;25: 1000–8.

[25] Li Y, Nagira T, Tsuchiya T. The effect of hyaluronic acid on insulin secretion in HIT-T15 cells through the enhancement of gap-junctional intercellular communications. Biomaterials 2006;27: 1437–43.

[26] Anderegg G, Flaschka H, Sallmann R, Schwarzenbach G. Metallindikatoren VII. Ein auf Erdalkaliionen ansprechendes Phatalein und sein analytische Verwendung. Helv Chim Acta 1954;37: 113–20.

[27] Yang L, Yamasaki K, Shirakata Y, Dai X, Tokumaru S, Yahata Y, et al. Bone morphogenetic protein-2 modulates Wnt and frizzled expression and enhances the canonical pathway of Wnt signaling in normal keratinocytes. J Dermatol Sci 2006;42:111–9.

[28] Kispert A, Vainio S, McMahon AP. Wnt-4 is a mesenchymal signal for epithelial transformation of metanephric mesenchyme in the developing kidney. Development 1998;125:4225–34.

[29] Kispert A, Vainio S, Shen L, Rowitch DH, McMahon AP. Proteoglycans are required for maintenance of Wnt-11 expression in the ureter tips. Development 1996;122:3627–37.

[30] Nery KYS, Rutlin ML, Radtke F, Fishell G, Gaiano N. Fibroblast growth factor receptor signaling promotes radial glial identity and interacts with Notch1 signaling in telencephalic progenitors. J Neurosci 2004;24:9497–506.

[31] Akai J, Halley PA, Storey KG. FGF-dependent Notch signaling maintains the spinal cord stem zone. Genes Dev 2005;19:2877–87.

日本臨牀　第65巻・第2号（平成19年2月号）別刷

特集：分子イメージング

原子間力顕微鏡（AFM）による蛋白質のイメージング

山越葉子　　中澤憲一　　土屋利江

方　法　論

原子間力顕微鏡(AFM)による蛋白質のイメージング

山越葉子[1]　中澤憲一[2]　土屋利江[3]

Protein imaging by atomic force microscopy

[1]Yoko Yamakoshi, [2]Ken Nakazawa, [3]Toshie Tsuchiya
[1]Associate Researcher, Department of Chemistry and Biochemistry, University of California at Santa Barbara
[2]Division of Pharmacology, [3]Division of Medical Devices, National Institute of Health Sciences

Abstract

Atomic force microscopy (AFM) has been used for imaging of non-conductive surface using a cantilever with a sharp probe to mediate the atomic force interaction between the probe and substrate. The application of AFM for the imaging of protein including transmembrane protein has been studied and revealed their single molecular structure on a nanometer scale. Especially for the transmembrane proteins that lack of 3D structural information obtained by X-ray crystallography, AFM imaging has significant advantages. Since the imaging is capable in the aqueous solution, the obtained images are expected to provide information that reflects structures found in the living cells. Additionally, the force curve measurement for intra- or inter-molecular non-covalent interaction such as protein folding or ligand-receptor interaction will be explained.

Key words: atomic force microscopy, protein imaging, recombinant $P2X_2$ receptor

1. 蛋白質の構造解析

生体の主要構成成分の一つである蛋白質は，生体内での有機化合物の代謝(酵素など)，情報伝達(受容体など)，組織骨格形成などにかかわる機能性分子であり，その機能に関連する構造の解析は現在の化学の分野で最もホットな分野の一つである．一般にアミノ酸配列を決定する一次構造解析は，繁用法があり，その結果から，α-ヘリックスやβ-シートなどの二次構造が推定される．しかし生体内での蛋白質の機能に大きくかかわっている三次元構造の決定は困難な点が多い．

現在行われている蛋白質三次構造決定法としては，X線結晶構造解析法と核磁気共鳴(nuclear magnetic resonance: NMR)分光法などがあげられる．X線解析法は解析対象とする蛋白質の単結晶を調製し，X線の照射回折を行い，三次元的画像を得るもので，解像度が非常に高い(Å レベル)という利点がある．特に近年の放射光を用いた測定法の開発により，解析される蛋白質の数は飛躍的に伸びた．しかし，本法は単

[1]カリフォルニア大学サンタバーバラ校　[2]国立医薬品食品衛生研究所薬理部　[3]同療品部

0047-1852/07/¥40/頁/JCLS

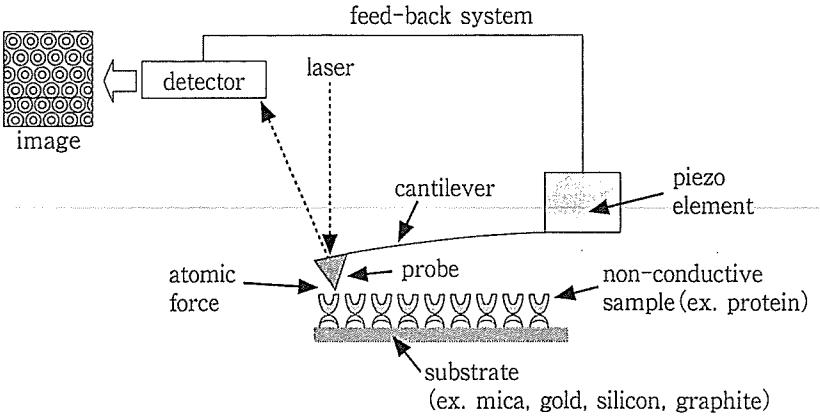

図1 原子間力顕微鏡(AFM)の模式図

結晶の調製が困難である難溶性の蛋白質の解析にはあまり向いておらず，また，得られる構造が結晶格子内における分子構造であるため，動的な構造ではなく，活性型の蛋白質の構造との相関には不明な点が残る．後者のNMR法は溶液中での測定法であり，生体内の蛋白質の挙動に近い情報を求めることが期待され，また，核オーバーハウザー効果(nuclear overhauser effect: NOE)などの手法を用いると，核の間の空間的距離の情報が得られ立体的構造に関する解析も可能である．ただし，蛋白質をNMRで測定して得られるスペクトルは，非常に複雑で解析が難しく，^{15}N-enrichした試料の調製が必要になる場合もある．また，試料としては高濃度溶液が必要であるため，難溶性あるいは微量しか発現していない蛋白質の解析にはあまり向いていない．

2. なぜ原子間力顕微鏡(AFM)で蛋白質の画像化を行うのか？

原子間力顕微鏡(AFM)を用いた蛋白質の解析の目的は蛋白質の大まかな構造と機能を知ることである．現在のところ，AFMの解像度はX線解析に遠く及ばない(大まかに言って1/10程度である)が，AFMを用いることの利点を以下にあげる．

(1) 試料の量が微量で済む．

(2) 高濃度溶液や単結晶の調製が不要である．

(3) 溶液中測定も可能であり，より生体内環境に近い条件下での測定が可能である．

(4) 経時的測定モードによりダイナミックな構造情報が得られる．

(5) 単一分子測定が可能である．

3. AFMからどんな情報が得られるのか？

a. 装置の概略とイメージング

AFMが最初に発表されたのは，1986年にPhysical Review Letters誌に掲載されたIBM-チューリヒの研究者達の報告[1]においてである．同研究グループはその数年前に，走査型トンネル顕微鏡(scanning tunneling microscope: STM)を発表し，原子像の画像化に成功しているが(1986年ノーベル物理学賞受賞)，トンネル電流を利用したSTM[2]が電導性のサンプルの測定のみに適用されるのに対し，AFMは非電導性のサンプルの測定も可能であり，DNAや蛋白質などの生体高分子の新しい解析手法として，威力を発揮することが期待されている．

機器の基本的な構造は，主に以下の4つの部分からなる(**図1**)．

(1) 試料の表面を走査する微細な探針(probe)

(2) 探針と試料表面との間に働く原子間力を増幅する微小な板ばね(cantilever)

(3) 探針および板ばねの高さや位置を調節する圧電(ピエゾ)素子

(4) 板ばねの変位を測定するレーザー光と，その反射を検出するフォトダイオード検出器

試料と原子間力を介して直接相互作用するのは板ばねに結合した探針の先端で，その位置制御は微細な圧電素子の動きによって行われ

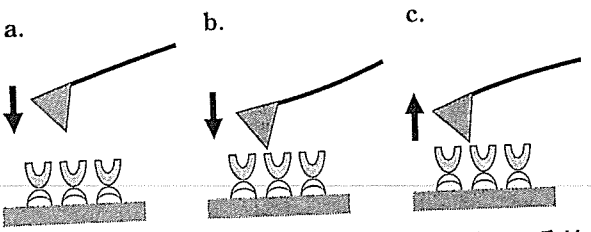

図2 AFM探針の試料の相互作用と板ばねのそり
a: 試料へ接近. b: 試料へ接触と, 板ばねのそり.
c: 試料からの離脱と原子間力による板ばねのそり.

る(図2). 試料表面にナノメーターレベルの距離で接近した板ばねは探針と試料との間に生じる原子間力に応じてそり(deflection)などの変位を起こす. そこにレーザー光を照射し, 生じる反射光を四分割フォトダイオードディテクターで検出し, その結果に基づきサンプルのトポグラフィカルな情報を画像化するのである. 具体的な蛋白質のイメージングの例は, 4. 測定法の項に後述する.

b. アンフォールディング

蛋白質の機能に大きくかかわる三次元構造は, 蛋白質のフォールディング(折りたたみ)により形成されるが, その機構に関しては未知の部分が多い. しかし, BSEに代表されるように蛋白質のミスフォールディングが疾患に関連している例が知られるようになり, フォールディングに関する基礎的知見は, 疾患の検出あるいは診断に重要な役割を果たすことが期待される.

ミュンヘン大学のGaubらのグループは, 膜貫通型蛋白質の一つバクテリオロドプシンを用いて, AFMによるアンフォールディングの実験を行った[3]. バクテリオロドプシン分子が多量に発現した*Halobacterium salinarum*の紫膜を劈開したばかりのマイカ表面上にマウントし, そこへAFM探針を接触させた後引っぱり上げると, フォースカーブに繰り返しパターンがみられた(図3). フォースカーブ上にピークが生じた距離と, フォールディングしているアミノ酸残基の長さは一致しており, ピークは蛋白質のフォールディングパターンを示していると考えられた.

c. 分子間相互作用の測定(chemical force microscopy)

ハーバード大学のLieberらは, AFM探針先端を特定の有機化合物で修飾し, 対象とする試料表面の官能基を選択的に検出しようとするchemical force microscopyを報告した[4]. 彼らは, 金で表面をコートしたシリコンナイトライド探針上に親水基(-COOH)あるいは疎水基($-CH_3$)を末端に有するアルキルチオール分子で自己組織化膜(self assembled monolayer: SAM)を形成させる方法でAFM探針の修飾を行い, フォースカーブ測定を行った(図4). その結果, CH_3/CH_3, CH_3/COOHおよびCOOH/COOH対での相互作用の違いをフォースカーブで検出することに成功した.

同様に, SAMで修飾したAFM探針を用いて, 分子のキラリティーの判別[5], 超分子ホストゲストコンプレックスの結合能の測定[6]などが報告されている. Gaubらのグループは, このchemical force microscopyをレセプター対リガンドの結合能測定に応用し, ストレプトアビジンとビオチンの結合能をフォースカーブとして測定した. この手法を種々のレセプター-リガンド対に応用することで, 将来的にはごく微量の蛋白質を用いたドラッグスクリーニング法として有用となる可能性も考えられる(図5).

4. 測定法(各論)

a. 試料の調製法

AFM測定において, 最も要となるところが, 試料の調製法である. 測定結果の良し悪しは, この試料調製法によるといっても過言でない. AFMは基本的にナノメーターレベルでの表面解析である. したがって, 測定する試料はできるだけ平坦なものである必要がある. 調製した試料の凸凹が激しいと, 単分子レベルでの測定を行う解像度が望めなくなるからである.

基板としては, マイカ, 単結晶金, グラファイトなどの原子レベルで平坦なものを用いる. マイカ, グラファイトは, 劈開したばかりのものを用い, 金は蒸着後高温でアニールし単結晶表面を形成したものを用いる. ここに目的の蛋

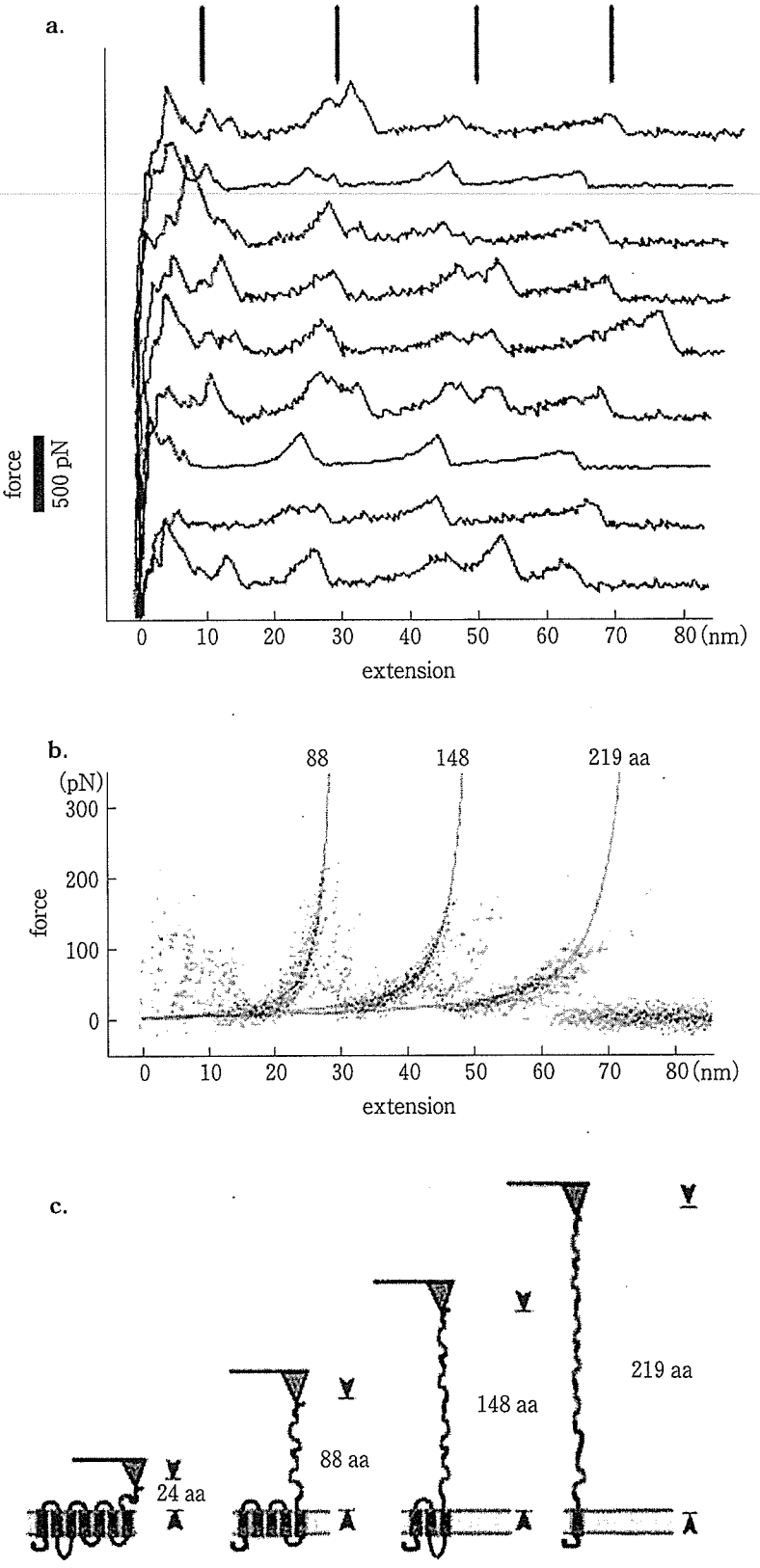

図3 AFMを用いた蛋白質アンフォールディングの実験

細胞膜中の膜蛋白質にAFM探針を接触(−1 nN, 1秒間)させ, C末端をAFM探針の先端に接着させる. それを引っ張ると, フォースカーブが生じ, カーブ上のピークまでの距離は, 予測されているフォールディングパターンのアミノ酸残基の長さと一致する.

(文献[3]より引用)

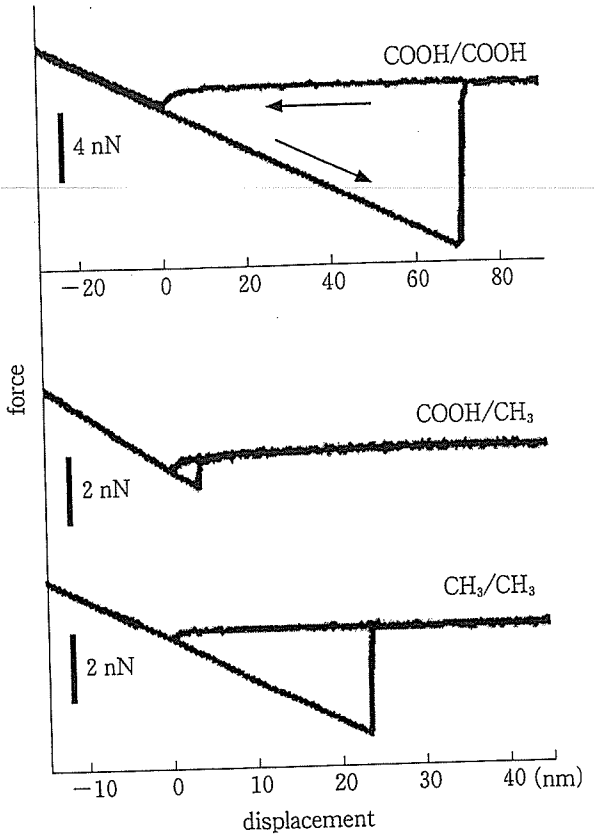

図4 末端に親水基あるいは疎水基を有する分子の自己組織化膜で修飾したAFM探針によるフォースカーブの測定
(文献[6]より引用)

白質を単分子膜として不動化させる．測定する蛋白質は，nativeなものを用いる場合もあれば，精製したものを用いる場合もある．膜結合型蛋白質では，細胞膜上に蛋白質が大量に発現していれば，それを直接測定することも可能であるが，精製した蛋白質を基板上に不動化したうえで測定する場合もある．測定は，溶媒を乾燥させたうえで行う場合と，溶液中でそのまま行う場合がある．いずれにしても超純粋な溶媒を用い，ほこりなどが基板に吸着しないような環境下で試料調製を行う必要がある．**図6**に調製法の異なる試料のイメージングの例を示す．乾燥した試料の大気中測定では蛋白質の凝集がみられたが，水溶液中での測定では，分散した蛋白質が単分子レベルで観測された．緩衝溶液中での測定では，蛋白質の再構築がよく観察され，チャネル孔らしき構造も観測された[7]．

b. 測　定

1) 測定モード

基本測定モードには，コンタクトモード，タッピングモード，ノンコンタクトモードの3種類があり(**図7**)，測定する試料に応じてモードを選択する必要がある．コンタクトモードは，探針の先端と試料を接触させながら測定する方法で，探針と試料の接触により生じる板ばねのそりをフィードバックシステムで一定に保つように設定し，電気的信号をもとに画像化する．スキャン速度を上げることができる，比較的凹凸の大きい試料の測定にも適しているなどの利点があるが，直接接触することにより試料に損傷が生じる可能性があるため，ソフトな試料(特に生物学的試料)の測定にはあまり適していない．これに対し，タッピングモードと，ノンコンタクトモードは一定の周波数で振動させた板ばねを用いた測定法である．タッピングモードでは，探針が試料に最も近づくときに軽く試料に接触するが，ノンコンタクトモードでは，全く接触しない．試料と探針が接近すると，相互作用により振動幅に変化が生じるが，これらのモードではフィードバックシステムにより振動幅を一定に保つよう調節し，その調節に必要な電気的信号をもとに画像化を行う．双方とも試料と探針の接触が少なく，ソフトな試料の測定に適している．

2) カンチレバー

AFMの解像度は探針の先端に依存する．すなわち，高分解能な測定のためには，探針の先端がなるべく微細であることが重要である．この微細加工が可能であること，更に，高い共振周波数を得られるという理由から，シリコン，シリコンナイトライドなどの素材が現在汎用されている．また，前述のchemical force microscopyなどの応用測定に用いられる，金コート済みの探針も市販されている．

更に高い解像度を達成するためには，探針の先端が非常に鋭利であることが求められ，単分子であることが理想である．より微細な探針素材としてはカーボンナノチューブを用いる研究も行われている[8]．

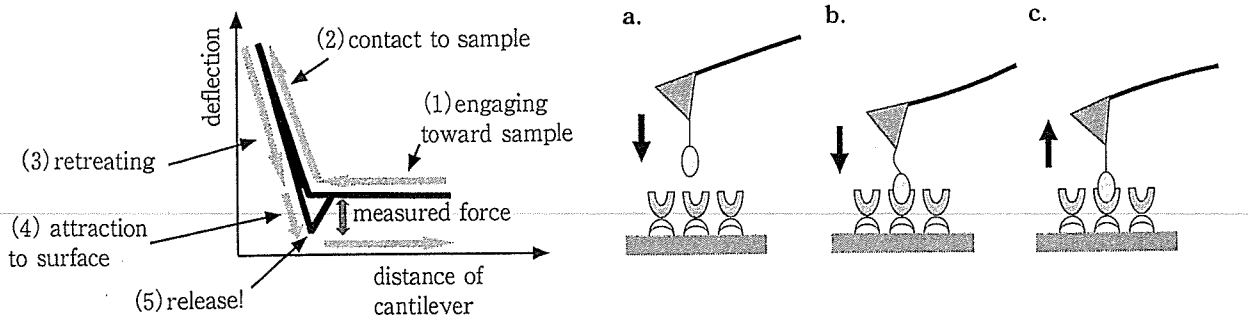

図5 Chemical force spectroscopyを用いたレセプターとリガンド間の分子間相互作用の実験
a: 試料に接近. b: 試料に接触. c: 相互作用(フォースとして現れる).

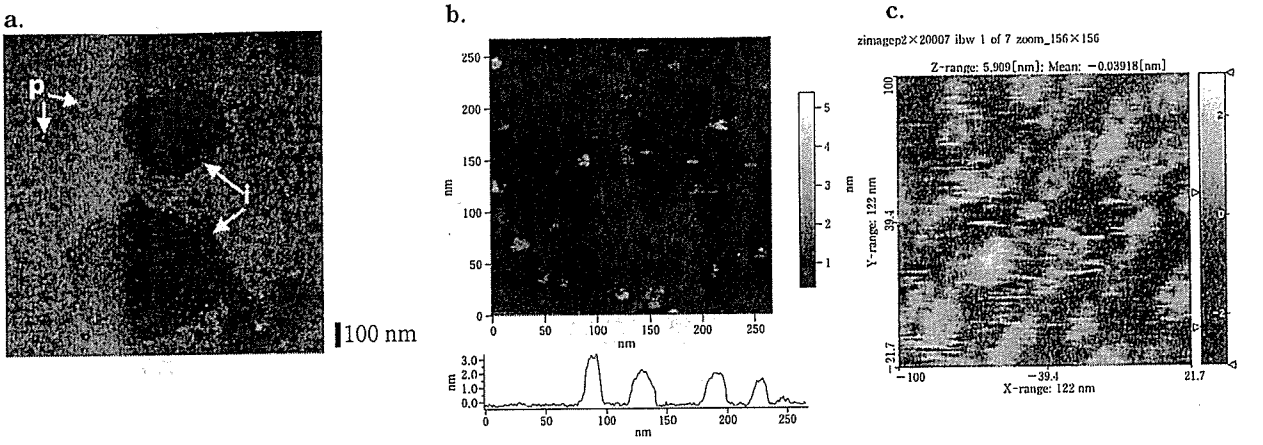

図6 膜蛋白質$P2X_2$受容体のAFMによるイメージング
a: 蛋白質水溶液をマイカ上に滴下後, 乾燥させたサンプルを測定した画像. 蛋白質が島状に凝集している状態が見える.
b: 蛋白質水溶液をマイカ上に滴下, そのまま水中で測定した画像とその断面図. 蛋白質が単分子状に分散している状態が見える.
c: 蛋白質の緩衝溶液をマイカ上に滴下, そのまま緩衝液中で測定した画像. 蛋白質が再構築し, チャネル状の構造を取っている状態が見える.

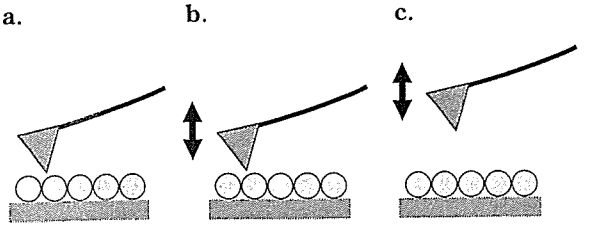

図7 AFMの測定モード
a: コンタクトモード. b: タッピングモード.
c: ノンコンタクトモード.

3) 膜結合型蛋白質のイメージングの例

難溶性で単結晶の作成が難しい膜蛋白質のイメージングにおいて, AFMが最も威力を発揮する. ドレスデン工科大学のMüllerらの研究グループは, 膜蛋白質のAFMイメージングを精力的に行っている. その成果の例を図8に示す.

図8は, Cx26 Hela細胞に多量に発現したコネキシン26分子を精製後, マイカ上にマウントして緩衝液中でAFM測定を行ったものである[9]. コネキシン分子の細胞外部分がサブ分子レベルで観測されている. コネキシン分子が六量体でチャネル孔を有する様子がわかる. 図8-aはカルシウムイオン非存在下, bは存在下での測定で, カルシウムイオンの添加により蛋白質のコンフォーメーションが変化し, チャネルの入り口の直径が1.5nmから0.6nmへと小さくなることが観測された.

図9は脂質二重膜中に埋包させた膜蛋白質

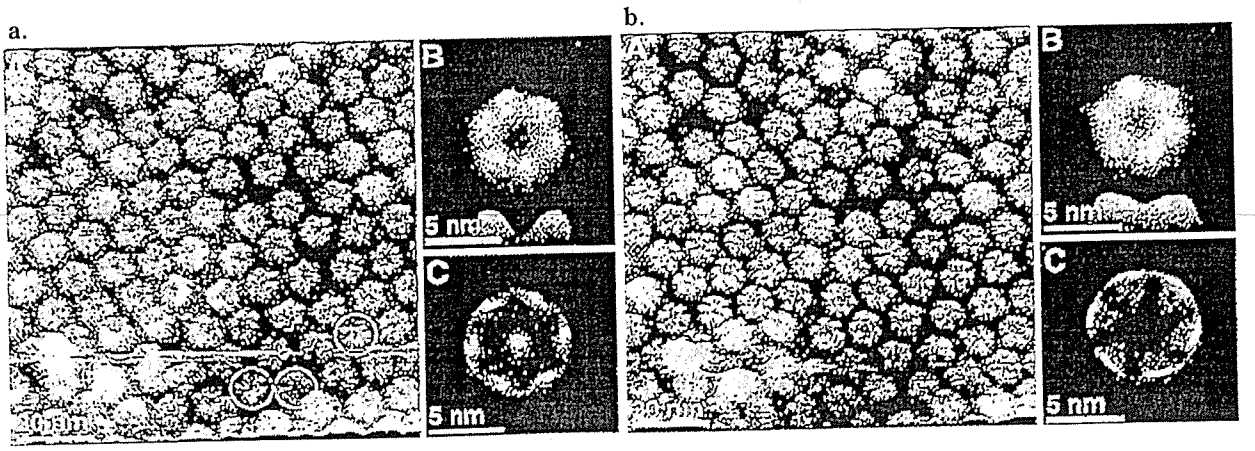

図8 コネキシン分子のAFMイメージ
a: Ca^{2+}非存在下での画像. b: Ca^{2+}存在下での画像. コンフォーメーションの変化がみられる.
(文献[9]より引用)

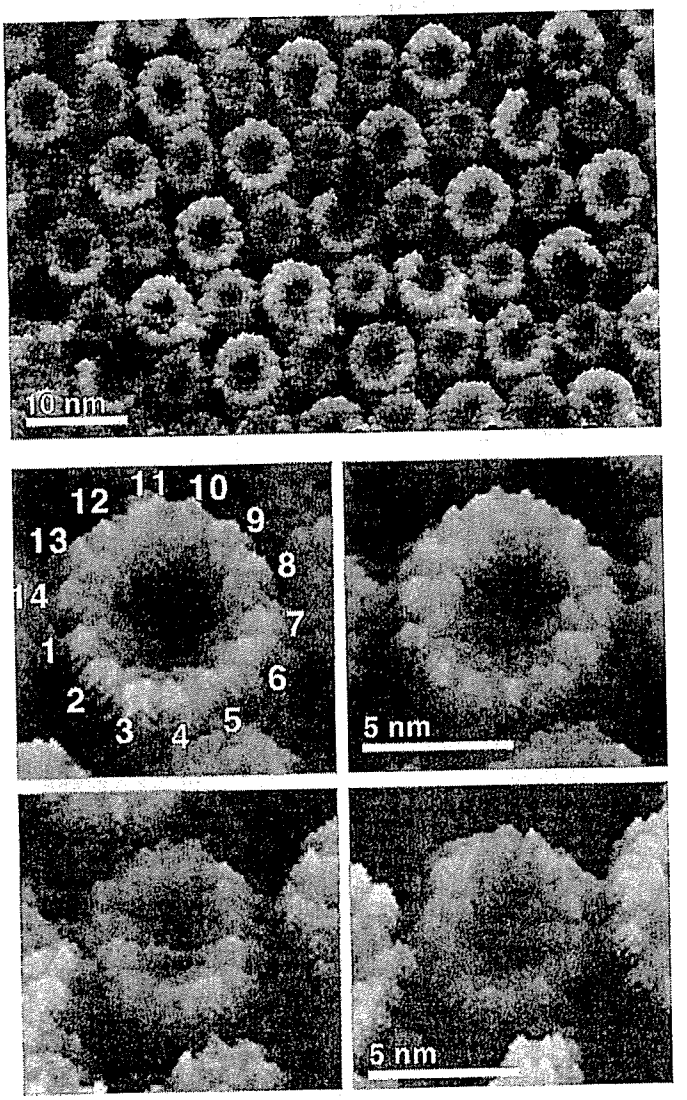

図9 精製後脂質二重膜中で再構築させたspinach chloroplast ATP synthaseのAFMイメージ
(文献[10]より引用)

のAFMイメージの例である[10,11]．精製したATP synthaseをdodecyl maltosideの存在下，フォスファチジルコリンおよびフォスファチジン酸と混合することで埋包させマイカ上で測定を行った．

5. 今後の進展

以上に紹介したように，AFMの生物試料への応用は主として膜蛋白質の解析に利用されている．これは，膜蛋白質の基板上での配向が均一であり，解析が行いやすいためである．膜蛋白質のX線結晶構造解析が酵素などの水溶性蛋白質より困難であることを考慮すれば，解像度は落ちるとはいえAFMの形状解析がこの種の蛋白質の研究に今後も有用であると予想される．また，X線による構造解析が既になされている蛋白質についても，AFMによる水溶液中の形状解析が動的構造について新たな知見をもたらす可能性が考えられる．

本稿では，単一蛋白質のイメージングの例を紹介したが，2種以上の蛋白質の水溶液中での会合状態を観察することも可能である．例えば，受容体とこれに直接的に働くエフェクター分子(G蛋白質など)との会合状態を観察することにより，生化学的応答の機構の可視化が可能となるかもしれない．

分子間相互作用の測定については，受容体とそのリガンド，酵素とその基質などの分子相互作用を1分子レベルで解析できれば，生体の分子メカニズムについて，これを力学的に解析するという全く新しい分野を切り開くことになるであろう．

文　献

1) Binning G, et al: Atomic force microscope. Phys Rev Lett **56**: 930-934, 1986.
2) Binning G, et al: Surface study by scanning tunneling microscopy. Phys Rev Lett **49**: 57-61, 1982.
3) Oesterhelt F, et al: Unfolding pathways of individual bacteriorhodopsins. Science **288**: 143-146, 2000.
4) Frisbie CD, et al: Functional group imaging by chemical force microscopy. Science **265**: 2071-2074, 1994.
5) McKendry R, et al: Chiral discrimination by chemical force microscopy. Nature **391**: 566-568, 1998.
6) Schönherr H, et al: Individual supramolecular host-guest interactions studied by dynamic single molecule force spectroscopy. J Am Chem Soc **122**: 4963-4967, 2000.
7) Nakazawa K, et al: Purification and aqueous phase atomic force microscopic observation of recombinant P2X2 receptor. Eur J Pharmacol **518**: 107-110, 2005.
8) Wooley AT, et al: Structural biology with carbon nanotube AFM probes. Chem Biol **7**: R193-R204, 2000.
9) Müller DJ, et al: Conformational changes in surface structure of isolated connexin 26 gap junctions. EMBO J **21**: 3598-3607, 2002.
10) Seelert H, et al: Proton-powered turbine of a plant motor. Nature **405**: 418-419, 2000.
11) Seelert H, et al: Fourteen protomers compose the oligomer III of the proton-rotor in spinach chloroplast ATP synthase. J Mol Biol **333**: 337-344, 2003.

J Artif Organs (2007) 10:22–28
DOI 10.1007/s10047-006-0363-y

ORIGINAL ARTICLE

Masato Tamai, PhD · Kazuo Isama
Ryusuke Nakaoka, PhD · Toshie Tsuchiya, PhD

Synthesis of a novel β-tricalcium phosphate/hydroxyapatite biphasic calcium phosphate containing niobium ions and evaluation of its osteogenic properties

Abstract To promote the osteogenic properties of osteoblasts, we synthesized a hydroxyapatite (HAp) with β-tricalcium phosphate (β-TCP) biphasic calcium phosphate containing Nb ions (NbTCP/HAp). NbTCP/HAp was prepared by annealing precipitates obtained by coprecipitation of an aqueous solution of $Ca(NO_3)_2$ and a mixture of $(NH_4)_2HPO_4$ and aqueous Nb solution. The precipitates can be regarded as a calcium-deficient HAp, the PO_4 sites of which are partly occupied by Nb ions. NbTCP/HAp was successfully synthesized by thermal decomposition of the precipitates. NbTCP/HAp enhanced the calcification of normal human osteoblasts (NHOst), and the amount of calcified tissue increased in proportion to the Nb ion concentration in the NbTCP/HAp. The alkaline phosphatase (ALP) activity of NHOst was also enhanced by NbTCP/HAp. Because Nb ions significantly enhance the ALP activity of NHOst, calcification by NbTCP/HAp is considered to be due to enhancement of ALP activity induced by Nb ions dissolved from NbTCP/HAp. These results indicate that NbTCP/HAp can be an effective bone repair material.

Key words Tissue engineering · Bone · Osteoblasts · Calcium phosphate · Nb ions

Introduction

Bone tissue engineering offers a promising alternative strategy for healing severe bone injuries by utilizing the body's natural biological response to tissue damage in conjunction with engineering principles. Osteogenic cells, growth factors, and biomaterial scaffolds form the foundation of the many bone tissue engineering strategies employed to achieve regeneration of damaged bone tissue. An ideal biomaterial scaffold will provide mechanical support to an injured site and also enhance osteogenic differentiation to encourage bone growth.[1] To develop biomaterial scaffolds with optimal performance, understanding the interactions between osteoblasts and scaffolds is extremely important.

Hydroxyapatite [HAp, $Ca_{10}(PO_4)_6(OH)_2$] and related calcium phosphate ceramics, e.g., β-tricalcium phosphate [β-TCP, β-$Ca_3(PO_4)_2$], have good biocompatibility with bone tissue because their chemical compositions are very similar to the mineral phase of human bone. It is well known that these calcium phosphate ceramics can be biologically bonded to natural bone. In fact, it has been reported that porous materials composed of HAp, β-TCP, or β-TCP/HAp biphasic calcium phosphate are useful for bone tissue regeneration because of their osteoconductivity.[2–6] It has also been reported that β-TCP/HAp biphasic calcium phosphate shows better osteoconductivity than HAp or β-TCP alone.[7,8] Therefore, this material has been actively studied for use as a scaffold for bone tissue regeneration.

In a previous study, Nb ions were reported to lower cytotoxicity[9] (IC_{50} of Nb ions for L929 fibroblasts is 3.63×10^3), and we reported that Nb ions significantly promoted the calcification of normal human osteoblasts (NHOst).[10] Furthermore, we succeeded in synthesizing a hydroxyapatite containing Nb ions (NbHAp) and showed that NbHAp has the potential to promote alkaline phosphatase (ALP) activity, an important factor in the generation of new bone, in NHOst.[11] In this study, to further promote the cell activity of osteoblasts, we synthesized β-TCP/HAp biphasic calcium phosphate containing Nb ions and investigated interactions between β-TCP/HAp biphasic calcium phosphate and NHOst in vitro.

Materials and methods

Synthesis and characterization of β-TCP/HAp biphasic calcium phosphate containing Nb ions

Reagent grade $Ca(NO_3)_2$, $(NH_4)_2HPO_4$, and $NbCl_5$ (Wako, Osaka, Japan) were used without purification. NbTCP/HAp

Received: May 26, 2006 / Accepted: September 28, 2006

M. Tamai · K. Isama · R. Nakaoka · T. Tsuchiya (✉)
Division of Medical Devices, National Institute of Health Sciences,
1-18-1 Kamiyoga, Setagaya-ku, Tokyo 158-8501, Japan
Tel. +81-3-3700-4842; Fax +81-3-3707-6950
e-mail: tsuchiya@nihs.go.jp

samples were prepared by annealing precipitates obtained from coprecipitation of an aqueous solution of $Ca(NO_3)_2$ with a mixture of $(NH_4)_2HPO_4$ and an aqueous solution of Nb as described below. $Ca(NO_3)_2$ and $(NH_4)_2HPO_4$ were completely dissolved in distilled water. The aqueous Nb solution was prepared by mixing distilled water and $NbCl_5$ dissolved in 5% hydroxyacetone and 5% 2-aminoethanol.[12] A 0.2 M $(NH_4)_2HPO_4$ aqueous solution was combined with 0.01 M $NbCl_5$ and stirred with a magnetic bar at Nb/(Nb + P) molar ratios of 0.0000, 0.0167, or 0.1667. The pH of the mixture was adjusted to 10 using 1N NaOH throughout the reaction, and 0.2 M $Ca(NO_3)_2$ was slowly dropped into the mixture (20 ml/min). The amount of 0.2 M $Ca(NO_3)_2$ solution was adjusted to a Ca/(Nb + P) molar ratio of 1.6 in order to synthesize β-TCP/HAp biphasic calcium phosphate, followed by stirring the suspension for 24 h at room temperature. The precipitates were centrifuged at 3600 rpm for 5 min and washed with distilled water. The resulting precipitates of Nb/(Nb + P) with molar ratios of 0.0000, 0.0167, and 0.1667 were named NbHAp-0, NbHAp-I, and NbHAp-II, respectively. These precipitates were then annealed at 800°C for 2 h (temperature increase: 5°C/min) and named NbTCP/HAp-0, NbTCP/HAp-I, and NbTCP/HAp-II, respectively. The NbTCP/HAp samples obtained were characterized by X-ray diffraction analysis (XRD, Rint2000, Rigaku, Tokyo, Japan) with Cu K_α radiation (40 kV, 50 mA). The XRD profiles of 2θ angles between 20° and 60° with a step interval of 0.01° were collected at a scanning rate of 4°/min. Also, measurement of the lattice parameter was carried out using the 211, 112, and 300 planes of HAp, and data for the lattice parameter were collected with a scan rate of 0.025°/min. The observed interplanar spacing was corrected using elemental Si as a standard material.

Concentrations of Ca, P, and Nb ions in the precipitate were estimated by inductively coupled plasma analysis (ICP, HP4500, Hewlett-Packard, CA, USA) after the precipitate was dissolved in HNO_3 solution. Microstructural evaluation of the precipitates was performed by scanning electron microscopy (SEM, JSM-5800LV, JEOL, Tokyo, Japan; acceleration voltage: 25 kV) and energy-dispersive X-ray spectroscopy (EDX) (LV5800, JEOL).

Osteogenic effects of NbTCP/HAp

NbTCP/HAp pellets were fabricated to investigate their effects on the osteogenic function of osteoblasts. In total, 100 mg of powdered NbTCP/HAp was put into a stainless steel mold and uniaxially pressed at 30 MPa for 1 min to form a pellet 0.5 mm in thickness and 12 mm in diameter. The pellets were sintered at 800°C for 2 h (temperature increase: 5°C/min).

NHOst were purchased from BioWhittaker (Walkersville, MD, USA) and maintained in d-minimumessential medium (αMEM) (Gibco, Grand Island, NY, USA) containing 10% fetal calf serum (FCS, Kokusai Sinyakyu, Tokyo, Japan) in incubators at 37°C in a humid atmosphere with 5% CO_2. All assays were performed using αMEM containing 10% FCS supplemented with 10 mM β-glycerophosphate.

Cells were seeded on the pellets as described below. Each NbTCP/HAp pellet was immersed in 1 ml culture medium in a well of a 24-well cell culture plate (Corning, Corning, NY, USA) and incubated at 37°C for 24 h. After discarding the medium, 300 μl of new culture medium was put into each well, followed by 1 ml of NHOst suspension (4×10^4 cell/ml), and incubation was carried out for 4 h. Finally, the cell-seeded NbTCP/HAp pellet was transferred to a new well of a 24-well plate with 1 ml of the test medium and incubated at 37°C in a humidified atmosphere with 5% CO_2 for 7–14 days.

Extracts from various NbTCP/HAp samples were prepared to investigate their effects on dissolved ions. NbTCP/HAp powder (100 mg/ml) was added to the culture medium (αMEM) containing 10% FCS and immersed at 37°C for 24 h. After changing the medium, the suspensions were stirred by a shaker at 200 rpm for 72 h at 37°C. The suspension was centrifuged at 3600 rpm for 5 min, and the supernatant was collected to use as an extract for an osteogenesis test in vitro. The atomic concentrations of Nb in the extract were measured by ICP.

An NHOst suspension (4×10^4 cells/ml) was added to culture wells and incubated for 4 h. After the NHOst had adhered to the well, the suspension medium was discarded and 1 ml of the extract supplemented with 10 mM β-glycerophosphate was added. The NHOst were incubated at 37°C in a saturated humid atmosphere with 5% CO_2 for 7–14 days.

We also examined the effect of Nb ions on the osteogenesis of NHOst. A solutionn of 0.2 μM $NbCl_5$/αMEM and serial dilutions were prepared. In addition to the experiment using the extracts indicated above, NHOst were cultured in $NbCl_5$/αMEM supplemented with β-glycerophosphate for 7–14 days.

Proliferation of NHOst cells in each experiment was estimated by a TetraColor One assay (Seikagaku, Tokyo, Japan), which incorporates an oxidation–reduction indicator based on detection of metabolic activity. After a 7-day incubation, the culture medium was discarded and 2% TetraColor One/αMEM solution was added to each well and was incubated for 2 h. The absorbance of the supernatant at 450 nm was measured using a μQuant spectrophotometer (Bio-tek, Winooski, VT, USA) to estimate the proliferation of the test cells. After estimating the proliferation, the cells were washed with phosphate-buffered saline [PBS(–)], followed by the addition of 1 ml of 0.1 M glycine buffer (pH 10.5) containing 10 mM $MgCl_2$, 0.1 mM $ZnCl_2$, and 4 mM *p*-nitrophenylphosphate sodium salt. The absorbance of the added buffer at 405 nm after 5 min incubation at room temperature was detected to evaluate the ALP activity of the test cells. After measurement of ALP, the NHOst cultured in the extract were washed with PBS(–) three times and the calcium phosphate deposited by NHOst was estimated. The amount of deposited calcium phosphate dissolved in 0.1 N HCl solution was determined by a Wako Calcium C test kit (Wako), which is based on the *o*-cresolphthalein complex color development method. The NHOst in all assays were stained in 5% Giemsa solution and observed by light microscopy (Nikon, Eclipse TE300, Tokyo, Japan) to confirm

Table 1. Chemical composition and characteristics of the precipitates prepared in this study

Sample	Phase	Annealing temperature	Theoretical composition[a]		Measured composition[a]		Color of precipitate	Lattice parameter[b]	
			Ca/(P + Nb)	Nb/(P + Nb)	Ca/(P + Nb)	Nb/(P + Nb)		*a*-axis (nm)	*c*-axis (nm)
NbHAp-0	HAp		1.60	0.000	1.60	–	White	–	–
NbHAp-I	HAp		1.60	0.017	1.56	0.013	Pale yellow	–	–
NbHAp-II	HAp		1.60	0.167	1.56	0.077	Buff yellow	–	–
NbTCPHAp-0	β-TCP + HAp	800°C	1.60	0.000	1.60	–	White	0.939	0.687
NbTCP/HAp-I	β-TCP + HAp	800°C	1.60	0.017	1.56	0.013	White	0.942	0.689
NbTCP/HAp-II	β-TCP + HAp	800°C	1.60	0.167	1.56	0.074	White	0.943	0.690

HAp, hydroxyapatite; NbHAp, hydroxyapatite containing Nb ions; TCP, tricalcium phosphate
[a]Molar ratio
[b]Lattice parameter for HAp

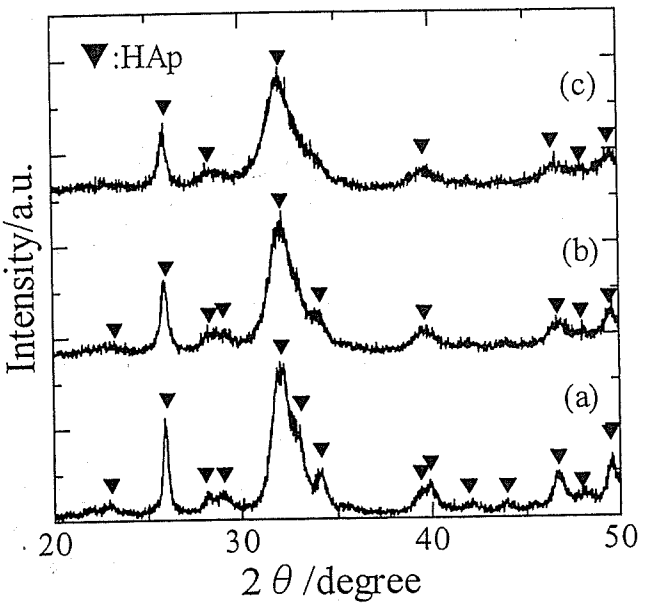

Fig. 1. X-ray diffraction (XRD) patterns of the precipitates with a Ca/(P + Nb) molar ratio of 1.50: *a*, Nb/(Nb + P) = 0; *b*, Nb/(Nb + P) = 0.0167; and *c*, Nb/(Nb + P) = 0.1667. *Triangles* represent XRD peaks due to the crystal structure of hydroxyapatite (HAp)

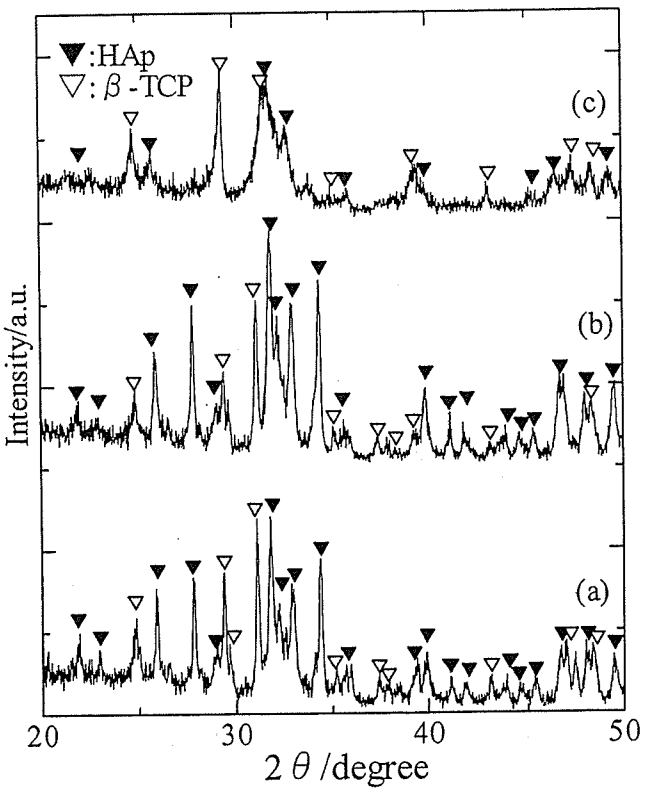

Fig. 2. XRD patterns of the annealed precipitates with a Ca/(P + Nb) molar ratio of 1.50: *a*, Nb/(Nb + P) = 0; *b*, Nb/(Nb + P) = 0.0167; and *c*, Nb/(Nb + P) = 0.1667. These precipitates were annealed at 800°C. *β-TCP*, β-tricalcium phosphate

their proliferation. All results were expressed as mean values ± SD and were analyzed statistically with Student's *t* test.

Results

XRD patterns of the precipitates prepared in this study are shown in Fig. 1. The XRD indicated that precipitates with Nb/(Nb + P) molar ratios from 0 to 0.167 had a monolithic apatite structure, irrespective of the Nb/(Nb + P) molar ratio of the starting solution, although the level of crystallite decreased as the Nb content increased. XRD patterns of the precipitates with various Nb/(Nb + P) molar ratios annealed at 800°C are shown in Fig. 2. The level of crystallites of the precipitates was high due to the annealing, and their diffraction peaks were composed of those of both HAp and β-TCP. Interestingly, the crystallite level decreased when the Nb level increased.

The chemical compositions and characteristics of the precipitates prepared in this study are summarized in Table 1. Both the Ca/(Nb + P) and the Nb/(P + Nb) molar ratios in precipitates measured by ICP approximately agreed with their theoretical values, except for the Nb/(P + Nb) molar ratio of NbTCP/HAp-II: the measured Nb/(P + Nb) molar ratio of NbTCP/HAp-II was 0.074, which is lower than the theoretical value of 0.167. The lattice parameter of the HAp phase in NbTCPHAp increased with increasing Nb content.

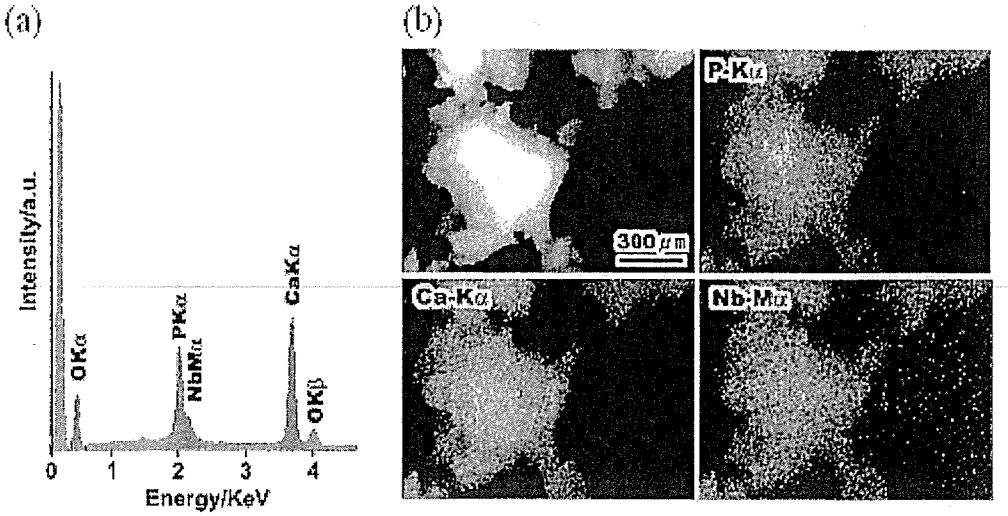

Fig. 3. Scanning electron microscopy–energy-dispersive X-ray spectroscopy spectra of NbTCP/HAp-II annealed at 800°C (**a**) and their mapping images from P-Kα, Ca-Kα, and Nb-Mα lines (**b**)

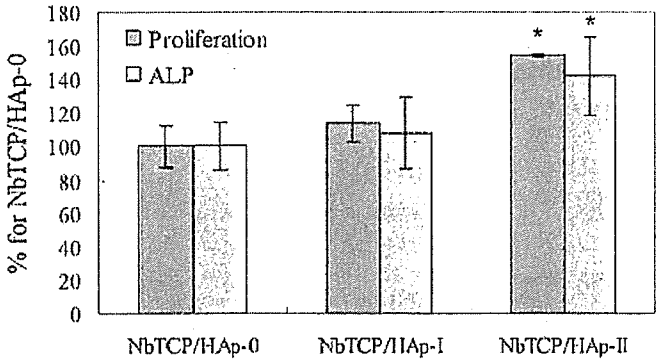

Fig. 4. Proliferation and alkaline phosphatase (*ALP*) activity of normal human osteoblasts (NHOst) cultured on various kinds of NbTCP/HAp pellets. *$P < 0.01$ against NbTCP/HAp-0 (without Nb ions)

The lattice parameters of NbTCP/HAp-0 without Nb ions were 0.939 nm for the *a*-axis and 0.687 nm for the *c*-axis, while those of NbTCP/HAp-II were 0.943 nm for the *a*-axis and 0.690 nm for the *c*-axis. In addition, the color of the precipitates became dark yellow as the Nb/(P + Nb) molar ratio increased, while the annealed precipitates of NbTCP/HAp were white.

SEM observation of the precipitates before annealing revealed that all precipitates were present as aggregates composed of primary particles of less than 1 μm in diameter, irrespective of the Nb/(P + Nb) molar ratio. Figure 3a shows SEM-EDX spectra of NbTCP/HAp-II. The EDX spectrum of Nb Mα was separated from the P K_α line and could be observed at 2.17 KeV, although its intensity was weak. The mapping images of the P-K_α, Ca-K_α, and Nb-M_α lines are shown in Fig. 3b. As shown in Fig. 3b, Nb ions were present at the same site as the Ca and P ions, suggesting that the Nb ions were homogenously distributed in the aggregates.

The proliferation and ALP activity of NHOst cultured on various kinds of NbTCP/HAp pellets is shown in Fig. 4. The proliferation of NHOst cultured on NbTCP/HAp-II pellets was approximately 60% higher than that on NbTCP/HAp-0 without Nb ions ($P < 0.01$). As shown in Fig. 5, many

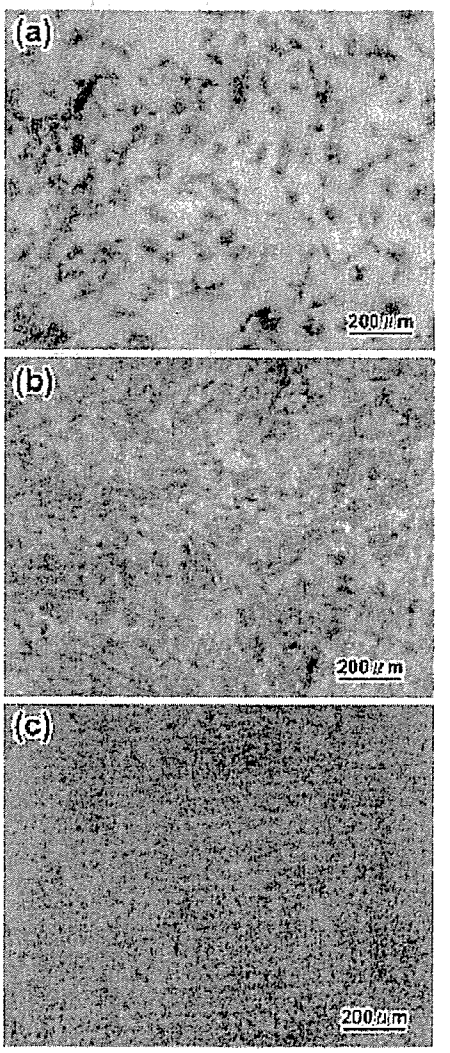

Fig. 5. Light microscopic images of NHOst cultured on various NbTCP/HAp samples for 7 days: *a*, NbTCP/HAp-0; *b*, NbTCP/HAp-I; and *c*, NbTCP/HAp-II. NHOst were stained by Giemsa solution

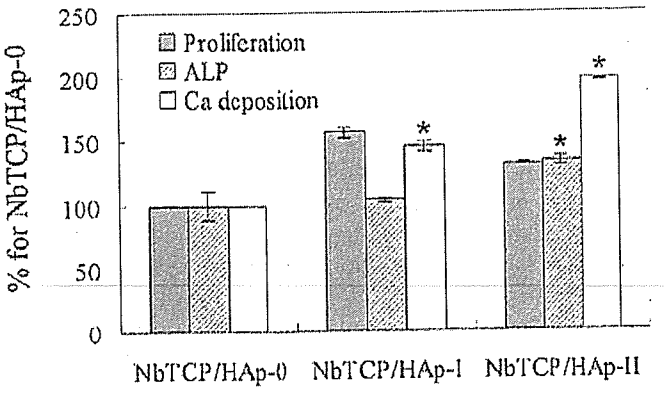

Fig. 6. Osteogenic properties (proliferation, ALP activity, and Ca deposition) of NHOst cultured in extracts from various NbTCP/HAp samples for 14 days. *$P < 0.01$ against NbTCP/HAp-0 (without Nb ions)

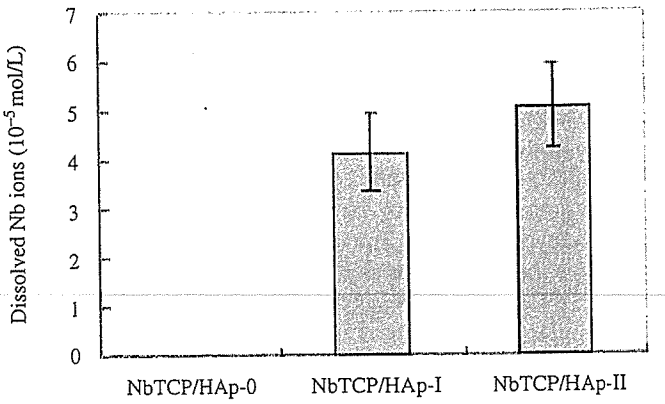

Fig. 7. Concentrations of Nb ions in extracts from various NbTCP/HAp samples. The concentration of Nb ions in cell culture medium was measured by inductively coupled plasma analysis

NHOst adhered to and spread on NbTCP/HAp-I and -II, while little spreading of NHOst was observed on HAp. In addition, as shown in Fig. 4, NHOst cultured on the NbTCP/HAp-II pellets expressed high ALP activity, compared with those cultured on NbTCP/HAp-0. Figure 6 shows the proliferation, ALP activity, and Ca deposition of NHOst cultured in extracts from various NbTCP/HAp samples for 14 days. Like the NHOst cultured on pellets, NHOst cultured in the extract from NbTCP/HAp-II expressed higher ALP activity than those in the extract from NbTCP/HAp-0. Furthermore, the amount of deposited calcium from NHOst increased with increasing Nb ion concentration in NbTCP/HAp, and the calcium deposition in the extract from NbTCP/HAp-II was twice that in the extract from NbTCP/HAp-0.

Figure 7 shows the concentration of Nb ions in extracts from NbTCP/HAp samples. It was found that Nb ions were released into the cell culture medium at concentrations of the order of 1×10^{-5} mol/l. To investigate the effect of Nb ions on NHOst function, NHOst were cultured in a medium containing Nb ions. The dependence of osteogenesis by NHOst on Nb ion concentration is shown in Fig. 8. Nb ions did not affect the proliferation of NHOst, but the ALP activity and Ca deposition of NHOst proceeded proportionally when the concentration of Nb ions was more than 1×10^{-5} mol/L.

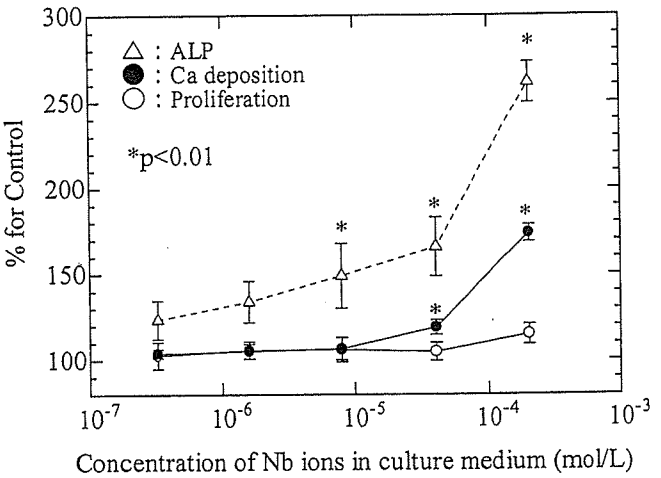

Fig. 8. Relationship between concentration of Nb ions in culture medium and osteogenic properties of NHOst. *$P < 0.01$ against cell culture medium without Nb ions

Discussion

Characterization of NbTCP/HAp biphasic calcium phosphate ceramics

As summarized in Table 1, before annealing the precipitates, the NbHAp samples were hydroxyapatite with low levels of crystallite. The hydroxyapatite structure is known to be very tolerant of ionic substitution.[12] Ca^{2+} ions, PO_4^{3-} ions, and OH^- ions can be replaced, partly or completely, by various cationic or anionic ions. Notably, as shown in Table 1, the lattice parameter of HAp increased when the Nb content in NbTCP/HAp was high. This fact suggests that Nb ions are taken into the apatite lattice. If a substitution of an Nb^{5+} ion for a Ca^{2+} ion in HAp occurred, the lattice parameter should decrease, since the ionic radius of Ca^{2+} and Nb^{5+} are 0.1 nm and 0.064 nm, respectively. Therefore, the possibility of substitution of Nb ions for Ca ions is low. On the other hand, although the structure of Nb ions in aqueous solution is not fully understood at present, it has been reported that Nb ions in solution are not present as Nb^{5+} but as niobiumate acid, $H_xNb_6O_{19}^{(8-x)-}$ ions (x = 0,1,2) for basic conditions,[14,15] and the niobiumate acid cluster ($H_xNb_6O_{19}^{(8-x)-}$) was polymerized or dissociated depending on the pH and ion concentration.[15] According to these reports, $H_4NbO_6^{3-}$ anionic monomer can exist in basal and low Nb concentrations (<0.08 M). Since the Nb concentration in this study was 0.01 M, Nb ions would exist as $H_4NbO_6^{3-}$ anionic monomers. $H_4NbO_6^{3-}$ may be substituted at the PO_4 site since the PO_4 site in HAp can be replaced by anionic

atomic groups. In addition, the ionic radius of the $H_4NbO_6^{3-}$ monomer and PO_4 are approximately 0.30 nm and 0.23 nm, respectively, suggesting that an increase in lattice parameter of NbTCP/HAp is ascribed to the substitution of PO_4 sites by this monomer in HAp. Furthermore, the fact that both the Ca/(Nb + P) and Nb/(P + Nb) molar ratios of the precipitates, as measured by ICP, approximately agreed with their theoretical values may support this hypothesis. Despite the theoretical Nb/(Nb + P) ratio being 0.1667, the Nb/(Nb + P) molar ratio in NbTCP/HAp-II was about 0.07, which suggests that the maximum amount of substituted Nb ions at the PO_4 site is around 0.07.

The Ca/(P + Nb) molar ratio in the NbHAp obtained in this study was lower than that of the stoichiometric value of 1.67 for HAp. Hydroxyapatite having a lower Ca/P molar ratio is known as calcium-deficient hydroxyapatite [Ca-def HAp, $Ca_{10-Z}(HPO_4)_Z(PO_4)_{6-Z}(OH)_{2-Z}$, Z = 0–1]. Therefore, NbHAp can be regarded as a Ca-def HAp in which the PO_4 sites are partly occupied by Nb ions.

Ca-def HAp decomposes to stoichiometric HAp and β-TCP at temperatures above 600°C according to the following reaction:[16,17]

$$Ca_{10-Z}(HPO_4)_Z(PO_4)_{6-Z}(OH)_{2-Z}\cdot nH_2O \rightarrow (1-Z)Ca_{10}(PO_4)_6(OH)_2 + 3Z\cdot\beta\text{-}Ca_3(PO_4)_2 + Z\cdot nH_2O$$

The above thermal decomposition reaction occurred during the annealing of NbHAp, resulting in a lower Ca/P molar ratio than the stoichiometric value of HAp because of partial β-TCP formation. In addition, the homogenously distributed Nb ions in NbTCP/HAp may result from thermal diffusion of Nb ions during the thermal decomposition process.

Osteogenesis of NHOst cultured on NbTCP/HAp

In this study, NbTCP/HAp showed potential to promote calcification of NHOst. This study indicated that osteogenic behavior of NHOst cultured on NbTCP/HAp pellets was consistent with that of NHOst cultured in extracts from the pellets, suggesting that dissolved ions from the NbTCP/HAp pellets affect calcification of NHOst. As shown in Fig. 7, Nb ions were apparently released from NbTCP/HAps and dissolved in the medium at concentrations of the order of 1×10^{-5} mol/l. When 4×10^{-5} mol/l of $NbCl_5$ was added to the culture medium, Ca deposition clearly increased (Fig. 8). Therefore, the enhancement of Ca deposition is considered to be due to the dissolved Nb ions. One possible mechanism for enhancement of calcification is discussed below.

ALP is known to play an important role in the calcification of bone.[18–20] Generally, the calcification of bone mineral occurs in the matrix vesicles budding from the surface of osteoblasts.[21] The nucleation of biological apatite, which is the initial stage of calcification, occurs due to the reaction between inorganic PO_4^{3-} ions produced by the ALP and calcium ions in matrix vesicles.

NHOst cultured on the NbTCP/HAp pellets containing Nb ions expressed high ALP activity compared with those cultured on HAp without Nb ion. Similarly, it was found that NHOst cultured in an extract from NbTCP/HAp containing Nb ions expressed higher ALP activity than those in the extract from HAp without Nb ions. These results suggest that Nb ions affect the enhancement of ALP activity. Based on the above calcification mechanism in matrix vesicles, the enhancement of calcification might result from the enhancement of ALP activity due to dissolved Nb ions from NbTCP/HAp. The enhancement of ALP activity increases the production of inorganic PO_4^{3-} ions, and then the inorganic PO_4^{3-} ions produced may be taken into the matrix vesicles. The subsequent nucleation of biological hydroxyapatite occurs due to a reaction of Ca ions and inorganic PO_4^{3-} ions, followed by calcification. Although we cannot deny that Nb ions directly promote calcification by NHOst unrelated with ALP expression, the essence of the calcification enhancement by NbTCP/HAp may be the enhancement of ALP activity by Nb ions dissolved from NbTCP/HAp. The biological effect of Nb ions on NHOst is under investigation. Although further studies are necessary to clarify the mechanism of enhanced calcification by Nb ions, this study strongly suggests that NbTCP/HAp is a more promising material for use as a bone tissue engineering scaffold than HAp.

Conclusion

In order to promote the osteogenicity of osteoblasts, we synthesized a combination of HAp and β-TCP biphasic calcium phosphate containing Nb ions (NbTCP/HAp). The NbTCP/HAp samples were prepared by annealing precipitates obtained by coprecipitation of an aqueous solution of $Ca(NO_3)_2$ with a mixture of $(NH_4)_2HPO_4$ and aqueous Nb solution. The precipitates obtained by the coprecipitation process can be identified as Ca-def HAp, the PO_4 sites of which are partly occupied by Nb ions. NbTCP/HAp samples were successfully obtained by thermal decomposition of the precipitates.

NbTCP/HAp enhanced calcification of NHOst. The enhancement of calcification of NbTCP/HAp was ascribed to the enhancement of ALP activity due to the dissolved Nb ions from NbTCP/HAp.

Acknowledgments This study was supported in part by a Grant-in-Aid for Scientific Research on Advanced Medical Technology from the Ministry of Labour, Health and Welfare of Japan, and a Grant-in-Aid from the Japan Health Sciences Foundation.

References

1. Service FR. Tissue engineers build new bone. Science 2000;289: 1498–1500
2. Tamai N, Myoui A, Tomita T, Nakase T, Tanaka J, Ochi T, Yoshikawa H. Novel hydroxyapatite ceramics with an interconnective porous structure exhibit superior osteoconduction in vivo. J Biomed Mater Res 2002;59:110–117
3. Ohgushi H, Goldberg VM, Caplan IA. Heterotopic osteogenesis in porous ceramics induced by marrow cells. J Orthop Res 1989;7: 568–578

A mouse strain difference in tumorigenesis induced by biodegradable polymers

Saifuddin Ahmed, Toshie Tsuchiya
Division of Medical Devices, National Institute of Health Sciences, 1–18-1 Kamiyoga, Setagaya-ku, Tokyo 158-8501, Japan

Received 13 November 2005; accepted 6 February 2006
Published online 10 August 2006 in Wiley InterScience (www.interscience.wiley.com). DOI: 10.1002/jbm.a.30753

Abstract: The use of poly-L-lactic acid (PLLA) surgical implants for repair of bone fractures has gained popularity in the past decade. The aim of this study was to evaluate the *in vivo* effect of PLLA plates on subcutaneous tissue in two mouse strains, BALB/cJ and SJL/J, which have higher and lower tumorigenicity, respectively. Gap-junctional intercellular communication and protein expression of connexin 43 were significantly suppressed, whereas secretion of transforming growth factor-β1 and expression of extracellular matrix, insulin-like growth factor binding protein 3, and cysteine-rich intestinal protein 2 were significantly increased in PLLA-implanted BALB/cJ mice when compared with BALB/cJ controls. Finally, tumors were formed after implantation of cultured cells from the more-tumorigenic BALB/cJ, but not SJL/J, mice into nude mice. © 2006 Wiley Periodicals, Inc. J Biomed Mater Res 79A: 409–417, 2006

Key words: poly-L-lactic acid; gap-junctional intercellular communication; transforming growth factor-β1; connexin 43; nude mice

INTRODUCTION

The morphologic, chemical, and surface electrical characteristics of a biomaterial can influence the extent of the cellular response to an implant,[1,2] but host factors also contribute, so that an identical material implanted in different species[3,4] or at different anatomical locations[5,6] may elicit different degrees of response. Poly-L-lactic acid (PLLA) is a synthetic degradable polymer with good biocompatibility that is widely used clinically for surgical implants and as a bioabsorbable suture material.[7,8] Long-term implants of PLLA produced tumors in rats,[9] and adverse effects were also reported in other animal experiments.[10] All tumors are generally viewed as the result of disruption of the homeostatic regulation of the cell's ability to respond to extracellular signals, which triggers intracellular signal transduction abnormalities.[11] During the transition from the single-cell organism to the multicellular organism, many genes evolved to regulate these cellular functions. One of these genes is the gene coding for a membrane-associated protein channel (the gap junction).[12] Gap-junctional intercellular communication (GJIC) involves two hemichannels or connexons,[13] and each connexon is composed of six basic protein subunits named connexin (Cx), which allow the cell–cell transfer of small molecules. Approximately 20 connexins are known, and they are expressed in a cell- and development-specific manner.[14,15] GJIC also plays an important role in the maintenance of cell homeostasis and in the control of cell growth.[16] Thus, disruption of GJIC has been shown to contribute to the multi-step, multi-mechanism process of carcinogenesis.[17–19] Several tumor-promoting agents have been shown to restrict GJIC by phosphorylation of connexin proteins, such as connexin 43, which is essential in forming the gap junction channel.[20,21] Our previous study revealed that PLLA increased the secretion of transforming growth factor-β1 (TGF-β1), suppressed the mRNA expression of Cx 43, and inhibited GJIC in the early stage after implantation, thus promoting tumorigenesis in BALB/cJ mice.[22] We have hypothesized that the difference in tumorigenic potentials of PLLA is caused mainly by the different tumor-promoting activities of these biomaterials and that TGF-β1 might have an important role in PLLA-implanted BALB/cJ mice. Therefore, in our present experimental approach, we aimed to determine the novel effects of PLLA plates in two mouse strains, BALB/cJ and SJL/J, after long-term implantation. Among mouse strains, the former is a more tumorigenic strain when compared with the later.[23]

Correspondence to: T. Tsuchiya; e-mail: tsuchiya@nihs.go.jp
Contract grant sponsors: Ministry of Health, Labour and Welfare and Japan Health Sciences Foundation